TOPOLOGICAL MATTER

Non-Abelian band topology in noninteracting metals

QuanSheng Wu[1,2], Alexey A. Soluyanov[3,4], Tomáš Bzdušek[5,6]*

Electron energy bands of crystalline solids generically exhibit degeneracies called band-structure nodes. Here, we introduce non-Abelian topological charges that characterize line nodes inside the momentum space of crystalline metals with space-time inversion ($\mathcal{PT}$) symmetry and with weak spin-orbit coupling. We show that these are quaternion charges, similar to those describing disclinations in biaxial nematics. Starting from two-band considerations, we develop the complete many-band description of nodes in the presence of $\mathcal{PT}$ and mirror symmetries, which allows us to investigate the topological stability of nodal chains in metals. The non-Abelian charges put strict constraints on the possible nodal-line configurations. Our analysis goes beyond the standard approach to band topology and implies the existence of one-dimensional topological phases not present in existing classifications.

Nodal-line metals (*1*–*11*) and nodal-chain metals (*12*–*20*) are crystalline solids that exhibit line degeneracies of electron energy bands near the Fermi energy. Although a large variety of such metals have been discussed to date, many of their properties remain unknown. Here, we find that a non-Abelian charge (i.e., topological invariant) of nodal lines (NLs) exists in the momentum ($\boldsymbol{k}$) space of metals with weak spin-orbit coupling (SOC) in the presence of $\mathcal{PT}$ symmetry [combination of time-reversal ($\mathcal{T}$) and space-inversion ($\mathcal{P}$) symmetry]. This non-Abelian topology in $\boldsymbol{k}$-space is fundamentally different from the non-Abelian exchange statistics of anyon quasiparticles in the coordinate space. It arises in the absence of interactions and superconductivity and governs the evolution of NLs in $\boldsymbol{k}$-space as the system parameters are continuously varied. In particular, the non-Abelian charge implies constraints on admissible NL configurations, including chains of intersecting NLs. We further find that materials hosting these topological excitations provide a $\boldsymbol{k}$-space analog of biaxial nematic liquid crystals, which exhibit non-Abelian disclination lines in coordinate space (*21*–*23*). On the basis of ab initio calculations, we predict that the discussed phenomena can be observed in readily available materials, in which the NL locations in $\boldsymbol{k}$-space can be manipulated by strain. This is illustrated with the example of elemental scandium (Sc). Additional details and mathematical considerations are provided in (*24*).

[1]Institute of Physics, École Polytechnique Fédérale de Lausanne, CH-1015 Lausanne, Switzerland. [2]National Centre for Computational Design and Discovery of Novel Materials MARVEL, École Polytechnique Fédérale de Lausanne (EPFL), CH-1015 Lausanne, Switzerland. [3]Physik-Institut, Universität Zürich, Winterthurerstrasse 190, CH-8057 Zurich, Switzerland. [4]Department of Physics, St. Petersburg State University, St. Petersburg, 199034 Russia. [5]Department of Physics, McCullough Building, Stanford University, Stanford, CA 94305, USA. [6]Stanford Center for Topological Quantum Physics, Stanford University, Stanford, CA 94305, USA.
*Corresponding author. Email: bzdusek@stanford.edu

Nodal lines in two-band models

We first consider NLs in two-band models. Although this problem was already addressed in (*1*–*20*), we use it here to set the stage for the discussion of non-Abelian topology in later sections.

Two-band Hamiltonians can be decomposed using the identity $\mathbb{1}$ and the Pauli matrices $(\sigma_x, \sigma_y, \sigma_z) = \boldsymbol{\sigma}$ as

$$\mathcal{H}_2(\boldsymbol{k}) = h_0(\boldsymbol{k})\mathbb{1} + \boldsymbol{h}(\boldsymbol{k}) \cdot \boldsymbol{\sigma} \qquad (1)$$

where $\boldsymbol{h}(\boldsymbol{k}) = (h_x(\boldsymbol{k}), h_y(\boldsymbol{k}), h_z(\boldsymbol{k}))$ are real functions of $\boldsymbol{k} = (k_x, k_y, k_z)$. In the absence of SOC we set $\mathcal{PT} = \mathcal{K}$ (complex conjugation), which removes σ_y from Eq. 1, making both $\mathcal{H}_2(\boldsymbol{k})$ and its eigenstates real (*3*). The Hamiltonian exhibits a NL at $\boldsymbol{k}$ if two conditions are fulfilled (*8*): $h_z(\boldsymbol{k}) = 0$ and $h_x(\boldsymbol{k}) = 0$.

To uncover the topological structure stabilizing these NLs, one needs to consider the space of available Hamiltonians (*9*). To emphasize an analogy with the theory of defects in ordered media (*23*), here we call it the order-parameter space. For later convenience, it is useful to encode Hamiltonians using their eigenstates. Assuming a $\boldsymbol{k}$-point that does not lie on a NL, we normalize the spectrum of the Hamiltonian in Eq. 1 to ±1 by taking

$$\mathcal{H}_2(\boldsymbol{k}) = \mathbb{1} - 2|u^o_{\boldsymbol{k}}\rangle\langle u^o_{\boldsymbol{k}}| \qquad (2)$$

where $|u^o_{\boldsymbol{k}}\rangle$ is the cell-periodic amplitude of the lower-energy Bloch state. Because this is a normalized two-component real vector, the order-parameter space is a circle (S^1). To be precise, one should note that both $\pm|u^o_{\boldsymbol{k}}\rangle$ encode the same Hamiltonian. However, removing this redundancy by identifying antipodal points of the S^1 still produces an S^1. Closed paths $\boldsymbol{\Gamma}$ in $\boldsymbol{k}$-space that avoid the NLs are characterized by the elements of the fundamental group (*9*, *23*, *24*) of the order-parameter space

$$w_{\boldsymbol{\Gamma}} \in \pi_1(S^1) = \mathbb{Z} \qquad (3)$$

By taking a path $\boldsymbol{\Gamma}$ that tightly encircles a NL, we can assign an integer winding number $w_{\boldsymbol{\Gamma}}$ (*11*) to the NL. Topological charges described by fundamental groups are calculated directly from the Hamiltonian and thus do not depend on the gauge of the eigenstates. However, in contrast to Wilson operators, the calculation of these topological charges requires fixing the basis of the underlying Hilbert space (*25*).

Nodal chains in two-band models

Before generalizing to models with more than two bands, we discuss the effects of a single mirror symmetry on NLs in two-band models. We reproduce some findings of (*12*–*20*), but also arrive at additional insights concerning the topological stability of intersecting NLs. We will show in the next section that some of these results are substantially altered in the presence of additional bands.

The presence of mirror symmetry $m_z : z \to -z$ represented by $\hat{m}_z = \sigma_z$ in the model of Eq. 1 forces $h_{x(z)}(\boldsymbol{k})$ to be an odd (even) function of k_z (*20*). For example (*26*)

$$h_x(\boldsymbol{k}) = k_x k_z \quad \text{and}$$
$$h_z(\boldsymbol{k}) = \pm k_x^2 + k_y^2 \pm k_z^2 - b^2 \qquad (4)$$

with $b = 2$ produces the NLs shown in Fig. 1, A to D (*15*). They all exhibit crossing points (CPs) of intersecting NLs. Expanding Eq. 4 around the CPs gives

$$h_x(\boldsymbol{k}) = k_x k_z \quad \text{and} \quad h_z(\boldsymbol{k}) \approx \pm k_y \qquad (5)$$

which describe a pair of mutually perpendicular intersecting NLs along $k_x = k_y = 0$ and $k_y = k_z = 0$.

Geometrically, we interpret the formation of intersecting NLs as follows (Fig. 1): A NL is produced when a cyan sheet defined by $h_z(\boldsymbol{k}) = 0$ crosses the orange sheet of $h_x(\boldsymbol{k}) = 0$, which, because of the m_z symmetry, is the plane $k_z = 0$. Intersections of cyan and orange sheets produce in-plane NLs. The existence of additional NLs that vertically cross the plane $k_z = 0$ requires that $h_x(\boldsymbol{k}) = 0$ on a pink sheet orthogonal to the plane. Such a pink sheet appears in the model of Eq. 1 when the product $\sigma_z h_x(\boldsymbol{k})$ changes sign. The out-of-plane NLs correspond to intersections of cyan and pink sheets. The CPs of in-plane and out-of-plane NLs correspond to three-sheet intersections. Breaking m_z symmetry leads to mixing of the orange and pink sheets, and causes a nontrivial separation of the CPs, as previously observed in (*10*, *20*). We illustrate this for $h_x(\boldsymbol{k}) = k_x k_z - \frac{1}{10}$ and $h_x(\boldsymbol{k}) = k_x k_z - \frac{k_y}{20}$ in Fig. 1, E and F.

Here, we explain the stability of CPs topologically using the relative homotopy approach of (*27*) (see fig. S1). The m_z symmetry reduces the space of available Hamiltonians (with normalized spectrum) inside the $k_z = 0$ plane to only two points, namely $\pm\sigma_z$. In-plane NLs separate regions with different $\hat{m}_z$ eigenvalues of $|u^o_{\boldsymbol{k}}\rangle$ (*5*), denoted $\lambda^o_{\boldsymbol{k}}$. This allows us to define a $\{+1, -1\} \cong \mathbb{Z}_2$ topological number $\nu_{\boldsymbol{k}_1,\boldsymbol{k}_2} = \lambda^o_{\boldsymbol{k}_1} \cdot \lambda^o_{\boldsymbol{k}_2}$ for any pair of in-plane momenta $\boldsymbol{k}_{1,2}$ (*7*). However, tracking the sign of $h_{x,z}(\boldsymbol{k})$ on a loop encircling an in-plane NL reveals that it also carries a nontrivial

$\mathbb{Z}$ charge defined by Eq. 3, i.e., it has an orientation. Notably, open-ended paths γ with endpoints $\partial\gamma$ inside the plane $k_z = 0$ can be assigned a winding number $w_\gamma \in \mathbb{Z}$ too, provided that $\nu_{\partial\gamma} = +1$ (*27*) (fig. S4). The closed composition of path γ with its mirror image $(m_z\gamma)^{-1}$, denoted $\mathbf{\Gamma}$, carries an even winding $w_\mathbf{\Gamma} = 2w_\gamma$. In the presence of mirror symmetry, CPs are protected by $|w_\gamma| = 1$ on a semicircular path γ enclosing the CP. The winding number $|n_\mathbf{\Gamma}| = 2$ on the closed path $\mathbf{\Gamma}$ remains meaningful even when the mirror symmetry is broken, and enforces the nontrivial separation of the CP seen in Fig. 1, E and F. The mismatch (*25*) between the $\mathbb{Z}$ winding number $w_\mathbf{\Gamma}$ and the $\mathbb{Z}_2$ invariant $\nu_{\partial\gamma}$ leads to conditions for creating a nodal chain by colliding in-plane NLs, as illustrated in Fig. 2. The relative orientation of NLs near a CP always follows the pattern observed in Fig. 2D.

Nodal chains in many-band models

We now demonstrate that the presence of additional bands modifies the topological stability of CPs. We illustrate this phenomenon by studying the spectrum of the Hamiltonian

$$\mathcal{H}_3(\boldsymbol{k}) = \begin{pmatrix} E_0 & tk_x & tk_z \\ tk_x & k_y & k_xk_z \\ tk_z & k_xk_z & -k_y \end{pmatrix} \qquad (6)$$

which augments the two-band model of Eq. 5 with an additional orbital with energy E_0, coupled to the two original orbitals with amplitudes proportional to t (we set $t = \frac{1}{2}$ throughout). The Hamiltonian of Eq. 6 has a mirror symmetry $\hat{m}_z = \mathrm{diag}(1, 1, -1)$ (*26*).

Assuming first that $E_0 > 0$, the NLs formed by the lower two bands (i.e., the original ones) of the Hamiltonian of Eq. 6 take the form of the red intersecting lines in Fig. 3A. These NLs intersect at a CP, similar to the two-band discussion around Eqs. 4 and 5. However, decreasing E_0 to a negative value results in a trivial separation of these NLs (red lines in Fig. 3C). Such a separation is impossible in two-band models. Nevertheless, the CP did not vanish completely; it is now at the intersection of the NLs formed by the upper two bands (blue lines in Fig. 3, A to C). The transfer of the CP to another pair of bands occurs at a topological transition at $E_0 = 0$ (Fig. 3B). The description of such a process requires a mathematical framework capable of capturing NLs between both pairs of bands simultaneously and goes beyond the established "tenfold way" classification of topological insulators and superconductors (*28*, *29*) based on K-theory (*30*).

Quaternion charges in many-band models

Motivated by the observations of the previous section, we develop the complete many-band description of NLs in $\mathcal{PT}$-symmetric models with weak SOC. We first formally derive the non-Abelian topology; the next section discusses the implications for NL configurations.

For $\boldsymbol{k}$-points with a nondegenerate spectrum, we deform N-band Hamiltonian $\mathcal{H}_N(\boldsymbol{k})$ such that it exhibits some standard set of band energies (e.g., $\varepsilon_j = j$ for $1 \le j \le N$; we assume $N \ge 3$). This generalizes Eq. 2 to

$$\mathcal{H}_N(\boldsymbol{k}) = \sum_{j=1}^{N} \varepsilon_j |u_\boldsymbol{k}^j\rangle\langle u_\boldsymbol{k}^j| \qquad (7)$$

Such a Hamiltonian is uniquely encoded by a frame $\{|u_\boldsymbol{k}^j\rangle\}_{j=1}^N$ of orthonormal N-component vectors, modulo transformations $|u_\boldsymbol{k}^j\rangle \mapsto -\langle u_\boldsymbol{k}^j|$. The order-parameter space M_N can be expressed as the space of right-handed frames [isomorphic to orthogonal group SO(N)], modulo a point group of π rotations flipping the sign of an even number of the frame elements. Geometrically, this is the space of all orientations of a generic N-dimensional ellipsoid. Notably, the $N = 3$

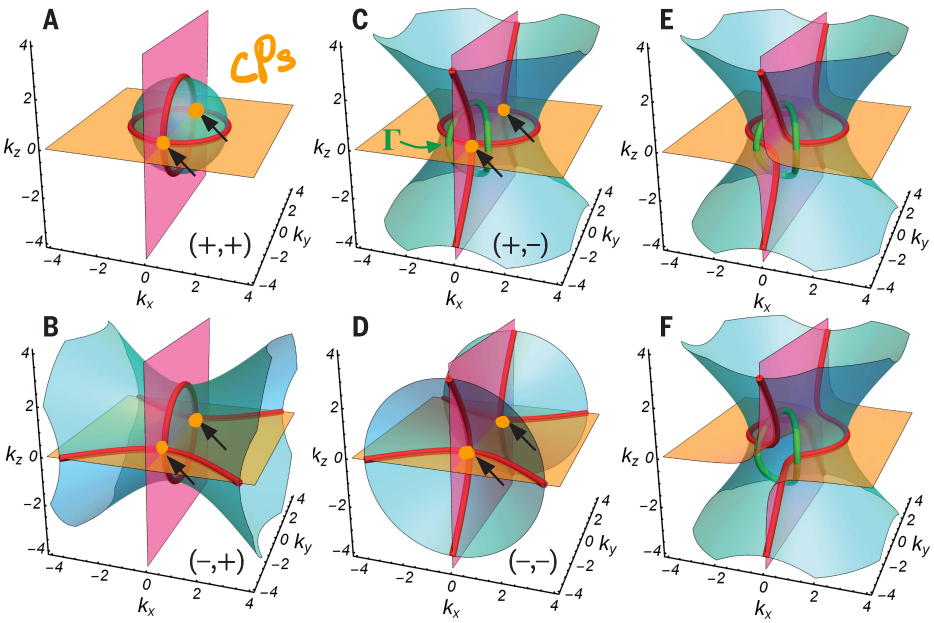

Fig. 1. Nodal lines in two-band models. Red lines indicate NLs of Hamiltonians of the form in Eq. 1. (**A to D**) For the Hamiltonian in Eq. 4 (with the indicated choice of ± signs in the expression for $h_z(\boldsymbol{k})$), NLs intersect at crossing points (black arrows), protected by a winding number $|w_\mathbf{\Gamma}| = 2$ on path $\mathbf{\Gamma}$ (green) shown in (C). (**E** and **F**) Upon breaking of the mirror symmetry, invariant $w_\mathbf{\Gamma}$ enforces a nontrivial separation of NLs into a pair of NLs that bend from vertical to horizontal.

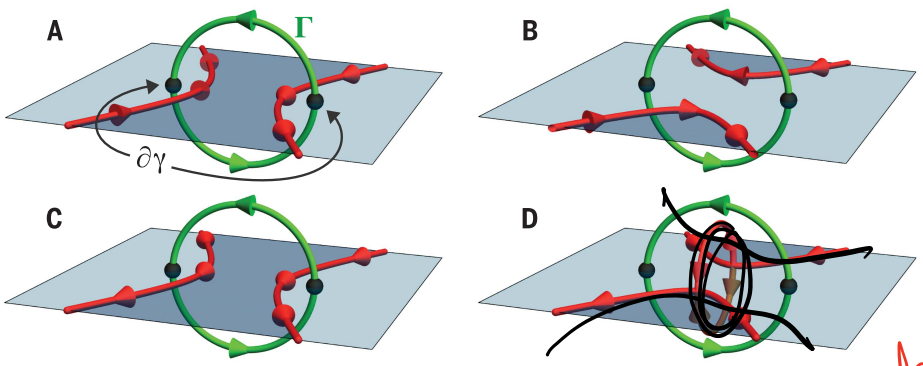

Fig. 2. Formation of intersecting nodal lines. Red lines indicate NLs of two-band Hamiltonians with a horizontal mirror-symmetry plane. Two shades of blue, separated by in-plane NLs, indicate regions with different mirror eigenvalue $\lambda_\boldsymbol{k}^\circ = \pm 1$ of the lower band, allowing us to define a $\mathbb{Z}_2$ charge. (**A**) Mirror-symmetric path $\mathbf{\Gamma}$ (green) encircles two in-plane NLs with opposite orientation, and crosses the plane at two points $\partial\gamma$ (black dots) with the same $\lambda_\boldsymbol{k}^\circ$. The pair of points $\partial\gamma$ carry a trivial value of the $\mathbb{Z}_2$ charge, and $\mathbf{\Gamma}$ carries zero value of the $\mathbb{Z}$ winding. Therefore, (**B**) in-plane NLs can trivially reconnect. (**C**) For an analogous setting with two parallel in-plane NLs, the $\mathbb{Z}$ winding becomes $|w_\mathbf{\Gamma}| = 2$, indicating that an obstruction must remain for shrinking path $\mathbf{\Gamma}$ to a point even after the reconnection of in-plane NLs takes places. (**D**) This implies the appearance of two out-of-plane NLs that are connected to the in-plane NLs.

case is mathematically equivalent to the order-parameter space of biaxial nematic liquid crystals (*21*). In these materials, molecules with an approximate ellipsoid symmetry have random positions but a frozen orientation.

Let us explicitly discuss the case $N = 3$. The order-parameter space is $M_3 = \mathrm{SO}(3)/D_2$, where D_2 is the three-dimensional "dihedral" crystallographic point group, which contains π rotations around three perpendicular axes, and the identity. Closed paths $\mathbf{\Gamma}$ in M_3 are characterized by the fundamental group of the order-parameter space, which is the quaternion group (*22*–*25*)

$$n_{\mathbf{\Gamma}} \in \pi_1(M_3) = \mathrm{Q} = \{\pm 1, \pm \mathrm{i}, \pm \mathrm{j}, \pm \mathrm{k}\} \quad (8)$$

with anticommuting imaginary units $\mathrm{i}^2 = \mathrm{j}^2 = \mathrm{k}^2 = -1$. The result in Eq. 8 is related to π rotation operators for spin-$\frac{1}{2}$ particles. The generalization of Eq. 8 to $N \geq 3$, discussed in (*24*), is closely tied to the symmetry of higher-dimensional Euclidean spaces (*31*, *32*).

The topological charge of Eq. 8 divides into five conjugacy classes: $\{+1\}$, $\{\pm \mathrm{i}\}$, $\{\pm \mathrm{j}\}$, $\{\pm \mathrm{k}\}$, $\{-1\}$. In analogy with the discussion below Eq. 3, considering a tight loop $\mathbf{\Gamma}$ that encircles a line defect allows us to label it by one of the five conjugacy classes. In biaxial nematics, the conjugacy classes involving the imaginary units describe three different species of disclination lines (*23*), as illustrated in fig. S8. In three-band crystalline solids, $\{\pm \mathrm{i}\}$ ($\{\pm \mathrm{k}\}$) characterize closed paths in $\boldsymbol{k}$-space that encircle a NL between the upper (lower) two bands, whereas $\{\pm \mathrm{j}\}$ corresponds to paths enclosing one of each species of NLs (*24*, *25*). The sign of the charge assigns an orientation to the NLs. Two NLs of the same orientation between the same pair of bands are described by $\{-1\}$. The green path in Fig. 3, A to C, belongs to this last conjugacy class, and the transfer of CP from the lower to the upper band gap corresponds to reinterpreting $-1 = \mathrm{k}^2$ as $-1 = \mathrm{i}^2$ (*24*). Note also that whereas $\mathrm{i}^2 = -1$ is nontrivial, $\mathrm{i}^4 = +1$ is trivial. We show in the supplementary text and in fig. S14 (*24*) that, indeed, a path enclosing four NLs of the same type and orientation can be continuously shrunk to a point without crossing a NL. The topological stability of CPs in the many-band case is addressed in the supplementary text and in fig. S15.

Constraints on nodal-line configurations

The quaternion group of Eq. 8 is non-Abelian. For example, the two species of NLs for $N = 3$ follow the rule $\mathrm{i} \cdot \mathrm{k} = -\mathrm{k} \cdot \mathrm{i} \neq \mathrm{k} \cdot \mathrm{i}$. We prove in (*24*) that such anticommutation property survives for $N \geq 3$, where it applies to NL pairs formed inside two consecutive band gaps. In this section, we show that the non-Abelian property poses constraints on admissible NL configurations.

Let us first consider a model with two mirror planes, $\hat{m}_z = \mathrm{diag}(1, 1, -1)$ and $\hat{m}_x = \mathrm{diag}(1, -1, 1)$, namely

$$\mathcal{H}_3(\boldsymbol{k}) = \begin{pmatrix} k_y^3 & tk_x & tk_z \\ tk_x & -k_y + (b + k_y^2) & ck_xk_z \\ tk_z & ck_xk_z & -k_y - (b + k_y^2) \end{pmatrix} \quad (9)$$

We set $t = 2$ and $c = \frac{1}{4}$ and study how the NLs (displayed as red and blue lines in Fig. 3, D to F) change when varying b. For $b > 0$, we find an extended NL formed by the lower (upper) pair of bands inside the $k_z = 0$ ($k_x = 0$) plane (Fig. 3D). Decreasing the value of b moves the two NLs toward each other, until they meet for $b = 0$ (Fig. 3E). The anticommutation relation implies that on the indicated green path, $n_{\mathbf{\Gamma}} = \mathrm{i} \cdot (-\mathrm{k}) \cdot (-\mathrm{i}) \cdot \mathrm{k} = -1$ (*23*, *24*). The nontrivial value of $n_{\mathbf{\Gamma}}$ forbids moving the NLs across each other (*33*) (fig. S12). Instead, we find that the extended NLs remain tangled for $b < 0$ via a link of two "earring" NLs (Fig. 3F), i.e., ring-shaped NLs attached to other NLs with only one CP. Such earring NLs have not been previously reported.

The anticommutation relation $\mathrm{i} \cdot \mathrm{k} = -\mathrm{k} \cdot \mathrm{i}$ can be interpreted as reversing the orientation of a NL each time it goes under a NL of the other species (*24*) (figs. S11 and S13). For example,

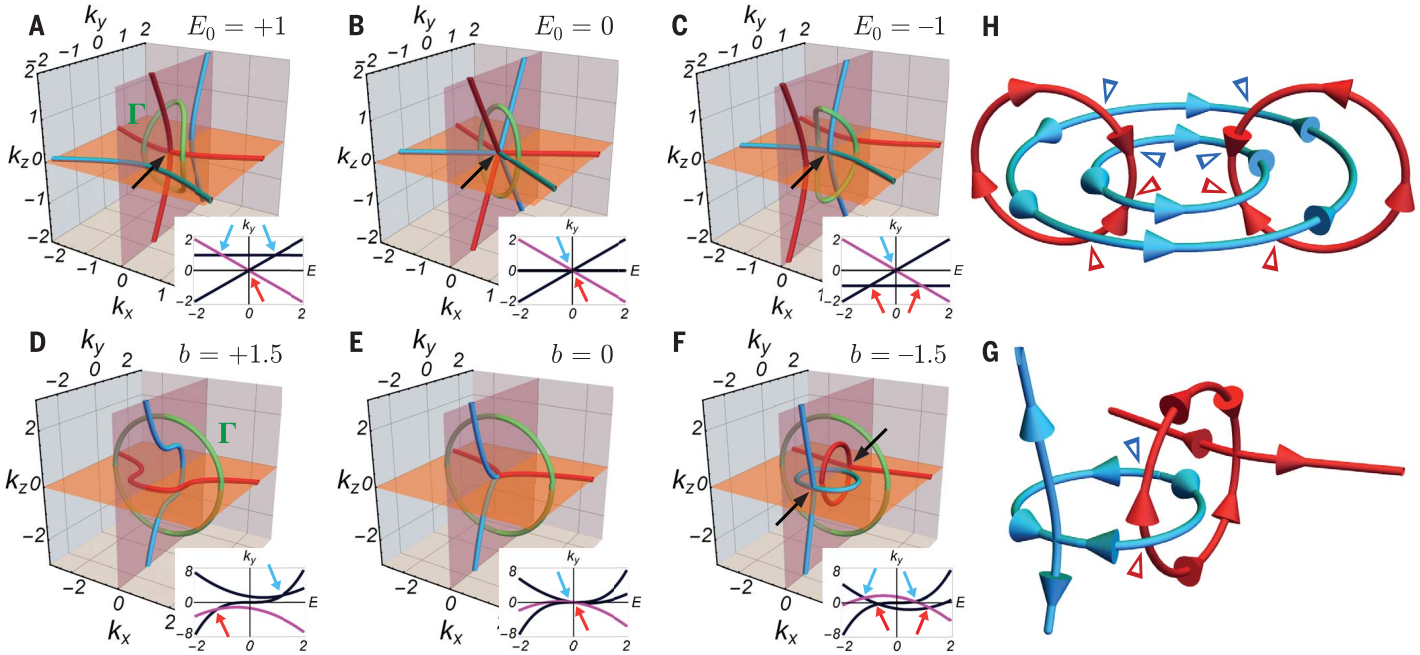

Fig. 3. Nodal lines in three-band models. For three-band Hamiltonians, we plot NLs formed by the lower (upper) two bands with red (blue) lines. (**A** to **C**) NLs of the model in Eq. 6 for three values of E_0. A crossing point (black arrows) is transferred between the two species of NLs when E_0 changes sign. The transfer follows from a quaternion charge $n_{\mathbf{\Gamma}} = -1$ on the green path. Insets show the spectrum along the $k_x = k_z = 0$ line, where black (magenta) bands carry positive (negative) $\hat{m}_z$ eigenvalue. (**D** to **F**) Analogous plots for the model in Eq. 9 for three values of b. Moving NLs of different species across each other results in the formation of "earring" NLs in (F). Such behavior is imposed by the quaternion charge $n_{\mathbf{\Gamma}} = -1$ on the green path. (**G**) The orientation of NLs in the configuration with linked "earrings". Owing to the non-Abelian group in Eq. 8, the orientation of a NL is reversed (indicated by triangular arrowheads) each time it goes under a NL of the other color (*24*). (**H**) An example of an admissible NL configuration involving linked rings. Each NL must enclose an even number of NLs of the other color.

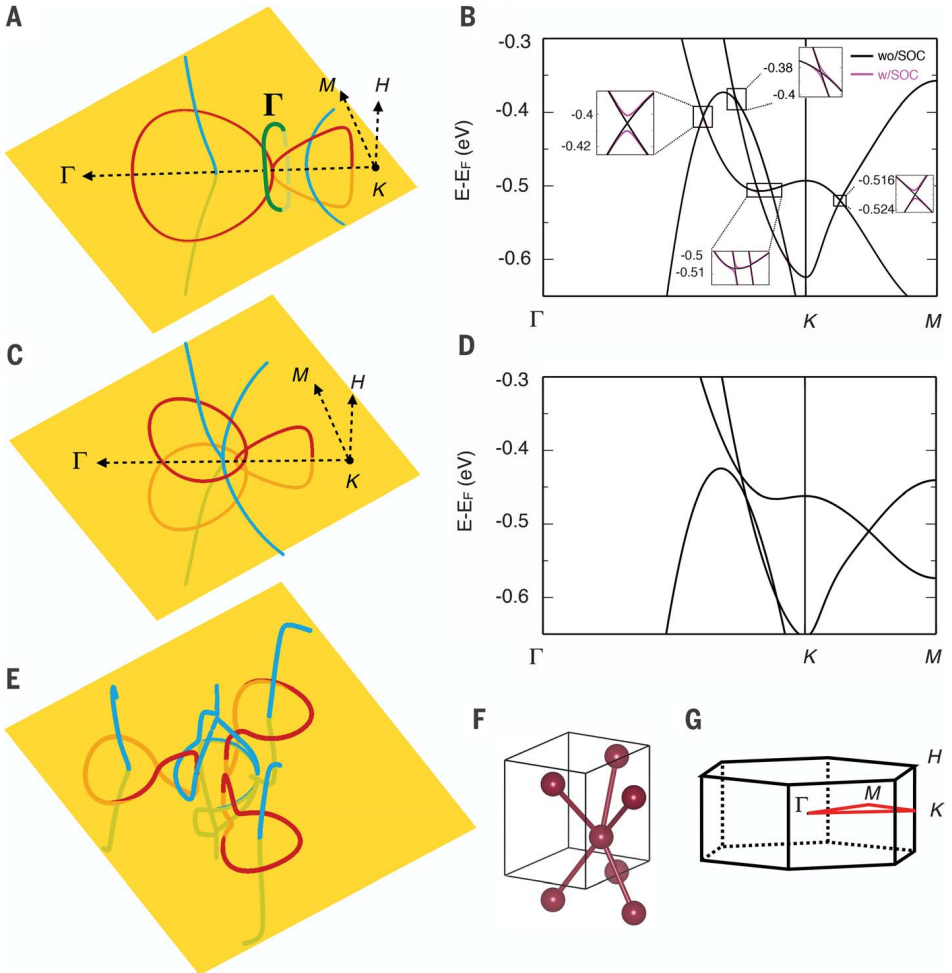

Fig. 4. Nodal lines of scandium (Sc). (**A**) Red (blue) NLs formed by the two lower (upper) of the three valence bands of Sc without SOC in the $k_z = 0$ plane (orange sheet). The red NLs exhibit a crossing point (CP) along the Γ*K* line, stabilized by the quaternion charge $n_{\mathbf{\Gamma}} = -1$ on the green path $\mathbf{\Gamma}$ (not to be confused with the BZ center point Γ). (**B**) The band structure of the three (six) valence bands of Sc along Γ*KM* without (with) SOC shown with black (magenta) colors. The SOC-induced splitting of the nodal lines (shown in insets) is less than 10 meV and is thus irrelevant when comparing calculations to ARPES results. (**C** and **D**) Evolution of the NLs and the band structure caused by a 2.25% biaxial tensile strain in the *x*,*y*-plane in the absence of SOC. The CP is now formed by the blue NLs, whereas the red NLs exhibit a pair of out-of-plane earrings. (**E**) NLs in the case of mirror-breaking compressive 1% strain in the $[10\bar{1}]$ direction. The CP has disconnected nontrivially. (**F**) The atomic unit cell of Sc. (**G**) The BZ of hexagonal Sc with its high-symmetry points. For a more detailed discussion and for additional ab initio data, see supplementary text and figs. S18 to S24 (*24*).

orientations of NLs in Fig. 3F follow the scheme in Fig. 3G. Consistency requires that NLs that are closed and isolated (i.e., without CPs) enclose an even number of NLs of the other species, such as in the example in Fig. 3H. Careful considerations of orientation reversals in many-band models can be used (*34*) to relate the monopole charges of NLs (*8*, *9*) to their linking structure (*10*). The orientation reversals also imply that the ability of two NLs to annihilate depends on the trajectory used to bring the NLs together, which we illustrate in fig. S10 of (*24*).

Topology in one dimension (1D) beyond the tenfold way

Given an *N*-band crystalline solid (assumed $\mathcal{PT}$-symmetric with weak SOC), the discussed non-Abelian topology ascribes to every closed path in $\boldsymbol{k}$-space (assumed to have a nondegenerate spectrum) an element of $\pi_1(M_N)$. For 1D systems, the Brillouin zone (BZ) itself forms such a closed path, allowing us to consider topological phases in 1D distinguished by a non-Abelian topological invariant $n_{\mathrm{BZ}} \in \pi_1(M_N)$. Band structures with $n_{\mathrm{BZ}} \neq +1$ cannot be adiabatically deformed into the Hamiltonian of uncoupled atomic orbitals (the atomic limit) unless we form a degeneracy between some pair of bands somewhere in the 1D BZ. These topological obstructions are stable against the addition of trivial bands (*24*).

Assuming $N \geq 3$ bands, the group $\pi_1(M_N)$ has $2^N = 2 \times 2^{N-1}$ elements, corresponding to the "doubled" point-symmetry group of an *N*-dimensional ellipsoid (*24*). The $\mathcal{PT}$ symmetry quantizes the Berry phase (*35*) of each band to 0 versus π (*8*, *36*). However, only $(N-1)$ of these phases are independent, because they must add up to 0 $(\mathrm{mod}\ 2\pi)$. Therefore, only 2^{N-1} elements of $\pi_1(M_N)$ are distinguished by Berry phases. The other 2^{N-1} elements correspond to composing the original 2^{N-1} elements with a (generalized) quaternion charge $n_{\mathbf{\Gamma}} = -1$. We show in (*24*) that for 1D paths with $n_{\mathbf{\Gamma}} = -1$, the Berry phase of each band is trivial 0. The computation of the generalized quaternion charges requires an augmentation of the Wilson loop technique (*37*–*40*) to spin bundles (*24*). We numerically investigate the edge states of these topological phases in the supplementary text and in figs. S16 and S17 (*24*).

Experimental signatures in scandium

The predicted properties of NLs derived from non-Abelian topology can be experimentally verified by using angle-resolved photoemission spectroscopy (ARPES) of elemental scandium (Sc) under strain. Sc has weak SOC and crystallizes in the hexagonal close-packed structure. Neglecting SOC (*24*), our ab initio calculations reveal that three valence bands of Sc form NLs plotted in Fig. 4, A and B, near the *K*-point of the BZ. Neglecting SOC, we observe a CP of two red "earring" NLs along the Γ*K* line, both threaded by a blue NL, in Fig. 4. As explained before, earring NLs are stabilized by the quaternion charge $n_{\mathbf{\Gamma}} = \mathrm{i} \cdot (-\mathrm{k}) \cdot (-\mathrm{i}) \cdot \mathrm{k} = -1$, which cannot be detected by measuring the Berry phase or Wilson loops. Therefore, experimental observation of earring NLs would provide indirect evidence of the non-Abelian topology. Although the weak SOC present in Sc opens a gap along the NLs, as shown in Fig. 4B and fig. S22, the induced NL splittings are smaller than 10 meV. Such small values are below the resolution of the best existing ARPES instruments; for this reason it is safe to neglect SOC in our discussion of Sc.

Applying a symmetry-preserving 2.25% biaxial tensile strain to Sc in the *x*, *y*-plane (*24*) moves the blue NLs together; we then observe a transfer of the CP from the red to the blue NLs (Fig. 4, C and D). Similar to Fig. 3, A to C, this transfer is also governed by $n_{\mathbf{\Gamma}} = -1$. Two additional out-of-plane earrings are developed by the red NLs in Fig. 4C; these are accidental, i.e., not imposed by the quaternion charge on any path. Note that elastic biaxial strain exceeding 2% is commonly achieved in epitaxially grown thin films of even more complicated compounds by using a lattice mismatch with the substrate; these films can be probed by ARPES spectroscopy (*41*, *42*) or x-ray scattering (*43*, *44*). To verify that ARPES measurements done on the biaxially stretched Sc thin film would illustrate our claims made for Sc bulk, we performed an ab initio calculation of subband splitting for a 30-nm-thick Sc thin film (*24*). We find this splitting to be ~5 meV (see fig. S24), which means that from the experimental point of view, this thin film represents the bulk band structure.

Finally, we consider a compressive 1% strain of Sc in the $[10\bar{1}1]$ direction, which breaks all the mirror symmetries (*24*). Such a distortion results in a nontrivial separation of CPs, compatible with the quaternion charge on path Γ in Fig. 4A. After the separation, the two red earring NLs of the unstrained case have merged into a single closed NL that encircles two blue NLs, compatible with the constraints discussed below Eq. 9. Observation of the NL configurations in Sc with and without strain would provide solid experimental support for the theoretical predictions made in this work.

Note added in proof: After the submission of this manuscript, a nontrivial exchange of band nodes in momentum space was conjectured for a class of 2D models using the mathematical technique of characteristic classes (*45*). A very recent work (*46*), which calls the quaternion charges introduced here "frame rotations," has generalized the non-Abelian topology to a class of 3D Weyl semimetals and has also related the technique of characteristic classes to the fundamental groups discussed in the present work.

REFERENCES AND NOTES

1. Y. Chen, Y.-M. Lu, H.-Y. Kee, *Nat. Commun.* **6**, 6593 (2015).
2. Y. Kim, B. J. Wieder, C. L. Kane, A. M. Rappe, *Phys. Rev. Lett.* **115**, 036806 (2015).
3. R. Yu, H. Weng, Z. Fang, X. Dai, X. Hu, *Phys. Rev. Lett.* **115**, 036807 (2015).
4. G. Bian *et al.*, *Nat. Commun.* **7**, 10556 (2016).
5. Y.-H. Chan, C.-K. Chiu, M. Y. Chou, A. P. Schnyder, *Phys. Rev. B* **93**, 205132 (2016).
6. L. M. Schoop *et al.*, *Nat. Commun.* **7**, 11696 (2016).
7. C. Fang, H. Weng, X. Dai, Z. Fang, *Chin. Phys. B* **25**, 117106 (2016).
8. C. Fang, Y. Chen, H.-Y. Kee, L. Fu, *Phys. Rev. B Condens. Matter Mater. Phys.* **92**, 081201 (2015).
9. T. Bzdušek, M. Sigrist, *Phys. Rev. B* **96**, 155105 (2017).
10. J. Ahn, D. Kim, Y. Kim, B.-J. Y. Yang, *Phys. Rev. Lett.* **121**, 106403 (2018).
11. A. A. Burkov, M. D. Hook, L. Balents, *Phys. Rev. B Condens. Matter Mater. Phys.* **84**, 235126 (2012).
12. T. Bzdušek, Q. Wu, A. Rüegg, M. Sigrist, A. A. Soluyanov, *Nature* **538**, 75–78 (2016).
13. S.-S. Wang, Y. Liu, Z.-M. Y. Yu, X.-L. Sheng, S. A. Yang, *Nat. Commun.* **8**, 1844 (2017).
14. R. Yu, Q. Wu, Z. Fang, H. Weng, *Phys. Rev. Lett.* **119**, 036401 (2017).
15. X. Feng, C. Yue, Z. Song, Q. Wu, B. Wen, *Phys. Rev. Mater.* **2**, 014202 (2018).
16. C.-J. Yi *et al.*, *Phys. Rev. B* **97**, 201107 (2018).
17. C. Gong, Y. Xie, Y. Chen, H.-S. Kim, D. Vanderbilt, *Phys. Rev. Lett.* **120**, 106403 (2018).
18. T. T. Heikkilä, G. E. Volovik, *New J. Phys.* **17**, 093019 (2015).
19. Z. Zhu, G. W. Winkler, Q. S. Wu, J. Li, A. A. Soluyanov, *Phys. Rev. X* **6**, 031003 (2016).
20. Q. Yan *et al.*, *Nat. Phys.* **14**, 461–464 (2018).
21. L. A. Madsen, T. J. Dingemans, M. Nakata, E. T. Samulski, *Phys. Rev. Lett.* **92**, 145505 (2004).
22. M. Kléman, L. Michel, G. Toulouse, *J. Phys. Lett.* **38**, 195–197 (1977).
23. N. D. Mermin, *Rev. Mod. Phys.* **51**, 591–648 (1979).
24. See supplementary materials.
25. Rotations of the basis of the Hilbert space may induce nontrivial automorphisms of the homotopy group. For example, the reordering of the basis orbitals of a two-band model (i.e., rotation by $R \propto \sigma_x$) flips the sign of the winding number in Eq. 3 [because it conjugates the complex quantity $h_x(\boldsymbol{k}) + ih_z(\boldsymbol{k})$] on all closed paths, thus leaving only the value $w_\Gamma = 0$ invariant. For the quaternion charge defined for three-band models in Eq. 8, only the charge values $n_\Gamma = \pm 1$ are invariant under all the possible automorphisms. This dependence on the choice of the basis does not influence the validity of our findings, e.g., it does not affect the (in)ability of two nodes to annihilate along a prescribed trajectory.
26. The models in Eqs. 4 to 6 also exhibit a second mirror symmetry $m_x : x \to -x$, which simplifies the form of the Hamiltonians. The symmetry m_x can be broken while preserving the validity of our arguments.
27. X.-Q. Sun, S.-C. Zhang, T. Bzdušek, *Phys. Rev. Lett.* **121**, 106402 (2018).
28. A. Kitaev, *AIP Conf. Proc.* **1134**, 22–30 (2009).
29. S. Ryu, A. P. Schnyder, A. Furusaki, A. W. W. Ludwig, *New J. Phys.* **12**, 065010 (2010).
30. P. Hořava, *Phys. Rev. Lett.* **95**, 016405 (2005).
31. M. F. Atiyah, R. Bott, A. Shapiro, *Topology* **3**, 3–38 (1964).
32. N. Salingaros, *J. Math. Phys.* **25**, 738–742 (1984).
33. V. Poenaru, G. Toulouse, *J. Phys. Lett.* **38**, 887–895 (1977).
34. A. Tiwari, T. Bzdušek, Non-abelian band topology of nodal-line rings in $\mathcal{PT}$-symmetric systems. arXiv:1903.00018 [cond-mat.mes-hall] (28 February 2019).
35. M. V. Berry, *Proc. R. Soc. London Ser. A* **392**, 45–57 (1984).
36. J. Zak, *Phys. Rev. Lett.* **62**, 2747–2750 (1989).
37. R. Yu, X. L. Qi, A. Bernevig, Z. Fang, X. Dai, *Phys. Rev. B Condens. Matter Mater. Phys.* **84**, 075119 (2011).
38. A. A. Soluyanov, D. Vanderbilt, *Phys. Rev. B Condens. Matter Mater. Phys.* **83**, 235401 (2011).
39. D. Gresch *et al.*, *Phys. Rev. B* **95**, 075146 (2017).
40. J. Baez, J. P. Muniain, *Gauge Fields, Knots, and Gravity* (World Scientific, Singapore, 1994).
41. P. D. King *et al.*, *Nat. Nanotechnol.* **9**, 443–447 (2014).
42. B. Burganov *et al.*, *Phys. Rev. Lett.* **116**, 197003 (2016).
43. S. Catalano *et al.*, *APL Mater.* **2**, 116110 (2014).
44. O. Ivashko *et al.*, *Nat. Commun.* **10**, 786 (2019).
45. J. Ahn, S. Park, B.-J. Yang, *Phys. Rev. X* **9**, 021013 (2019).
46. A. Bouhon, R.-J. Slager, T. Bzdušek, Non-Abelian reciprocal braiding of Weyl nodes. arXiv:1907.10611 [cond-mat.mes-hall] (24 July 2019)
47. G. Kresse, J. Furthmüller, *Phys. Rev. B Condens. Matter* **54**, 11169–11186 (1996).
48. Q. Wu, S. Zhang, H.-F. Song, M. Troyer, A. A. Soluyanov, *Comput. Phys. Commun.* **224**, 405–416 (2018).
49. A. A. Mostofi *et al.*, *Comput. Phys. Commun.* **185**, 2309–2310 (2014).
50. Q.-S. Wu, A. A. Soluyanov, T. Bzdušek, Supplementary Data for "Non-Abelian band topology in noninteracting metals," Materials Cloud Archive (2019).

ACKNOWLEDGMENTS

We thank A. Broido, J. Chang, M. Gibert, S. A. Kivelson, G. De Luca, X.-Q. Sun, A. Tamai, F. Valach, G. E. Volovik, and S.-C. Zhang for valuable discussions. We also thank the reviewers for their useful comments, which helped us to improve the clarity of the manuscript. **Funding:** Q.W. acknowledges the support of NCCR MARVEL. A.A.S. acknowledges the support of NCCR MARVEL, NCCR QSIT, and SNSF Professorship grants, and of Microsoft Research. T.B. was supported by the Gordon and Betty Moore Foundation's EPiQS Initiative, grant GBMF4302. **Author contributions:** T.B. had the initial idea, carried out the theoretical analysis, and led the project. Q.W. identified Sc as an illustrative material and performed the first-principle studies. T.B. and A.A.S. wrote the manuscript. **Competing interests:** The authors declare that they have no competing interests. **Data and materials availability:** Schematic illustrations and plots for the two-band and three-band models were generated using Wolfram Mathematica (version 11.3). To obtain the ab initio study of Sc with and without strain, we performed first-principle calculations as implemented in software Vienna Ab initio Simulation Package (VASP) (*47*). The nodal-line configurations are obtained by an open-source software, WANNIERTOOLS (*48*), based on the tight-binding models constructed by VASP+WANNIER90, where WANNIER90 (*49*) is an open-source software. Details are discussed in section VI of (*24*). We have made the Wolfram Mathematica files; the VASP, WANNIER90, and WANNIERTOOLS input files for the computation of band structures and nodal-line configurations of Sc; and the numerically obtained band-structure data publicly available on Materials Cloud Archive (*50*).

SUPPLEMENTARY MATERIALS

science.sciencemag.org/content/365/6459/1273/suppl/DC1
Supplementary Text
Figs. S1 to S24
References (*51*–*73*)

27 July 2018; accepted 14 August 2019
Published online 29 August 2019
10.1126/science.aau8740

Science

Non-Abelian band topology in noninteracting metals

QuanSheng Wu, Alexey A. Soluyanov and Tomás Bzdusek

Science **365** (6459), 1273-1277.
DOI: 10.1126/science.aau8740originally published online August 29, 2019

The topology of line nodes

Band structure degeneracies in topological materials can take the form of lines or even chains of interconnected loops. Wu *et al.* study theoretically these nodal lines and how they evolve as the system parameters are varied. They focus on a class of materials that have weak spin-orbit coupling and that respect a combination of inversion- and time-reversal symmetry. Noncommutative topological charges are associated with nodal lines in such materials that place constraints on the configurations of these lines. Calculations indicate that elemental scandium under strain may provide a test system for this unconventional topology.

Science, this issue p. 1273

Science (print ISSN 0036-8075; online ISSN 1095-9203) is published by the American Association for the Advancement of Science, 1200 New York Avenue NW, Washington, DC 20005. The title *Science* is a registered trademark of AAAS.